**Annals Geol. Surv. Egypt. XXXIX. (2022). pp. 57 - 80**

# RUNOFF WATER HARVESTING OPTIMIZATION USING RS, GIS AND WATERSHED MODELING IN WADI EL-ASSIUTI, EASTERN DESERT, EGYPT

**BY**

. El-Sayed, A. M [(1)], Elewa, H. H. [(1)], Abdel Wahed, M. [(2)], and Abu Salem, H. S. [(2)]

[(1)] Department of Water Resources, National Authority for Remote Sensing & Space Sciences (NARSS), Egypt.

[(2)] Department of Geology, Faculty of Science, Cairo University, Cairo, Egypt.

## Abstract

*Water in dry areas is a critical resource needed for developmental activities. Runoff water harvesting (RWH) will have its own bearing in combating water scarcity in the study area. The present work introduces a detailed hydro-morphometric analysis for El-Assiuti watershed in the northeastern desert to highlight the potentiality areas for the RWH. Hydro-morphometric parameters were delineated by analyzing ASTER DEM 30m and Landsat OLI+8 images. Eight thematic layers, i.e., basin area, basin slope, basin length, drainage density, maximum flow distance, length of overland flow, basin infiltration number, and volume of annual flood (calculated by SCS-CN method), were used to construct a multi-parametric weighted spatial probability model (WSPM). These thematic parameters, which include the linear, aerial, and relief aspects, were determined for the nine sub-watersheds of Wadi El-Assiuti. The WSPM was run two times for two scenarios: (1) equal weights are assigned for criteria and (2) weights are assigned according to the sensitivity analysis. The resulted RWH potentiality map classified El-Assiuti watershed into five classes ranging from very low to very high. Depending on the justified weights of thematic layers of scenario II, the very high RWH potentiality class is occupied by small parts in the northeastern and southeastern sides of the wadi with spatial distribution about 4 % relative to the total area of the wadi, while the high class is occupied by small zones in the northeastern, northwestern, and southeastern parts of the wadi with spatial distribution about 8 % relative to the total area of the wadi. Accordingly, the justified scenario II could be considered as a product of high reliability for determining the RWH potentiality, where it also coincides with the local inhabitants' experiences and needs.*

**Keywords:** Remote sensing, Watershed morphometry, GIS weighted spatial probability modeling, Runoff water harvesting, Wadi El-Assiuti, Eastern Desert, Egypt.

## INTRODUCTION

Wadi El-Assiuti constitutes part of the Eastern Desert which is one of the most significant wadis in middle Egypt which is a natural extension of Assiut Governorate. It represents one of the most promising desert areas for sustainable development where groundwater can be extracted. It is a dry drainage basin, whose main channel is 186 km in length (Elewa, 2008). The study area lies on the eastern bank of the Nile River northeast of Assiut governorate between latitudes 27° 00' - 27° 45' N and longitudes 30° 15' - 32° 30' E (Fig.1).

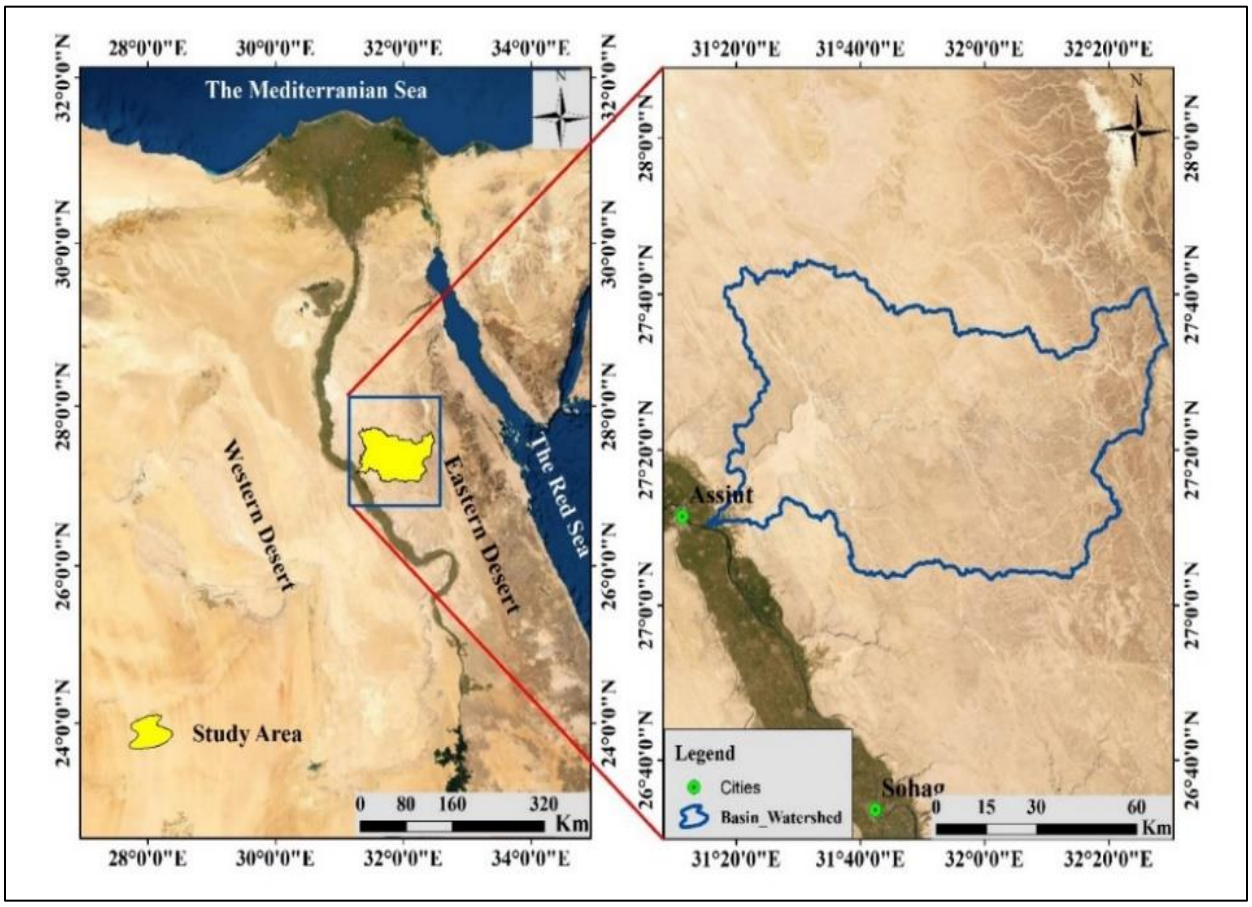


**Fig. (1): Location map of the study area.**

Wadi El-Assiuti is running in a desert area, however, its soil is highly potential for agricultural development if irrigation water is available. Accordingly, the investigation of the potential water resources in this area is crucial to meet the increased demands for water. The scarcity of water in the study area is the main obstacle for sustaining the development activities. The finding of new research tools or techniques for water exploration and conservation becomes a necessity.

From the climate data, Egypt is a part of the great desert belt that stretches eastward from the Atlantic across the whole North Africa and onwards through Saudi Arabia; like all the other lands lying within this belt, it is characterized by a warm and almost rainless climate (UNESCO, 1965). According to the Prediction of Worldwide Energy Resources NASA (POWER) Project data, the maximum rainfall storm occurred in February (1981) with an annual average amount of 24 mm (Fig. 2 and Table 1).

**Table (1): Amount of rainfall in the study area in the period from 1981 to 2020, (according to NASA POWER Project data, 2021). The amount in mm.**

| YEAR | JAN | FEB | MAR | APR | MAY | JUN | JUL | AUG | SEP | OCT | NOV | DEC | ANN (mm/year) |
|---|---|---|---|---|---|---|---|---|---|---|---|---|---|
| 1981 | 1.84 | 17.4 | 0.89 | 0 | 0.24 | 0.03 | 0 | 0 | 0 | 0.86 | 2.67 | 0.19 | 24.13 |
| 1982 | 5.99 | 3.05 | 0.33 | 2.55 | 0.98 | 0 | 0 | 0 | 0.03 | 0.01 | 1.27 | 0.03 | 14.24 |
| 1983 | 0.91 | 0.06 | 0.44 | 0 | 0 | 0 | 0 | 0 | 0 | 0.04 | 0 | 0.36 | 1.81 |
| 1984 | 0.07 | 0.03 | 0.83 | 0 | 0 | 0 | 0 | 0 | 0 | 0 | 1.73 | 0.04 | 2.71 |
| 1985 | 0.09 | 0.13 | 2.84 | 0.01 | 0.01 | 0 | 0 | 0 | 0 | 0 | 0.2 | 1.73 | 5.02 |
| 1986 | 0.06 | 0.17 | 0.22 | 0.22 | 0 | 0.04 | 0 | 0 | 0.02 | 12.67 | 3.1 | 1.01 | 17.5 |
| 1987 | 0.23 | 0.25 | 1.96 | 0.06 | 0.18 | 0 | 0 | 0 | 0 | 0.06 | 0 | 2.75 | 5.49 |
| 1988 | 0.56 | 0.11 | 0.22 | 0.01 | 0 | 0 | 0 | 0 | 0 | 0.01 | 0.02 | 1.56 | 2.49 |
| 1989 | 3.58 | 0.09 | 0.2 | 0.09 | 0 | 0 | 0 | 0 | 0 | 0 | 0.02 | 0.04 | 4.02 |
| 1990 | 1.99 | 1.85 | 3.87 | 0.02 | 0.39 | 0 | 0 | 0 | 0 | 0 | 0 | 0 | 8.11 |
| 1991 | 2.76 | 0.21 | 7.17 | 0.11 | 0.04 | 0 | 0 | 0 | 0 | 0 | 0.05 | 0.55 | 10.88 |
| 1992 | 0.84 | 1.89 | 0.31 | 0 | 1.51 | 0.23 | 0 | 0 | 0 | 0 | 0.03 | 1 | 5.81 |
| 1993 | 1.08 | 0.39 | 0.01 | 0 | 0.17 | 0 | 0 | 0 | 0 | 0.22 | 0 | 0.15 | 2.02 |
| 1994 | 0.46 | 0.04 | 0.83 | 0 | 0 | 0 | 0 | 0 | 0.01 | 0.26 | 5.53 | 0.32 | 7.47 |
| 1995 | 0.48 | 0.99 | 0.77 | 0.01 | 0.13 | 0 | 0 | 0 | 0 | 0 | 0.01 | 0.03 | 2.42 |
| 1996 | 0.32 | 0.06 | 0.13 | 0.02 | 0.06 | 0 | 0.03 | 0 | 0 | 0 | 1.77 | 0.02 | 2.42 |
| 1997 | 1.06 | 0.6 | 6.26 | 0.13 | 0.07 | 0 | 0 | 0 | 0.05 | 0.14 | 0 | 0.1 | 8.4 |
| 1998 | 0.1 | 0.36 | 0.09 | 0 | 0.21 | 0 | 0 | 0 | 0 | 0 | 0.01 | 0.16 | 0.92 |
| 1999 | 0.32 | 1.57 | 0.07 | 0 | 0 | 0 | 0 | 0 | 0 | 0 | 0 | 0.01 | 1.98 |
| 2001 | 0.18 | 0.06 | 0.23 | 3.49 | 0.01 | 0 | 0 | 0 | 0 | 0 | 0.01 | 0.16 | 4.13 |
| 2002 | 1.77 | 0.97 | 0.01 | 0 | 0 | 0 | 0 | 0 | 0 | 0.24 | 0.01 | 0.13 | 3.13 |
| 2003 | 0.24 | 0.07 | 0.13 | 0 | 0.13 | 0 | 0 | 0 | 0 | 0 | 0.09 | 1.32 | 1.98 |
| 2004 | 2.16 | 3.17 | 0.34 | 0 | 0 | 0 | 0 | 0 | 0 | 0 | 0.03 | 0.04 | 5.75 |
| 2005 | 0.58 | 2.33 | 1.36 | 0.03 | 0 | 0 | 0 | 0 | 0 | 0 | 0.01 | 0.01 | 4.33 |
| 2006 | 0.02 | 0.09 | 0.6 | 0.05 | 0.01 | 0 | 0 | 0 | 0 | 0.01 | 0 | 0.06 | 0.84 |
| 2007 | 0.03 | 0.69 | 0.08 | 0.62 | 0 | 0 | 0 | 0 | 0 | 0.08 | 0 | 0.2 | 1.7 |
| 2008 | 7.17 | 0.12 | 0 | 0 | 0 | 0 | 0 | 0 | 0 | 0.35 | 0 | 0 | 7.65 |
| 2009 | 0.02 | 0.21 | 0.03 | 0 | 0.01 | 0 | 0 | 0 | 0 | 0.01 | 0.01 | 0.01 | 0.3 |
| 2010 | 0.82 | 0.3 | 0.01 | 0 | 0.52 | 0 | 0 | 0 | 0 | 0 | 0 | 3.77 | 5.43 |
| 2011 | 8.61 | 0.04 | 0.04 | 0.03 | 0 | 0 | 0 | 0 | 0 | 0 | 0.24 | 0.01 | 8.97 |
| 2012 | 0.21 | 0.08 | 0.04 | 0 | 0.13 | 0 | 0 | 0 | 0 | 0 | 3.93 | 0.95 | 5.35 |
| 2013 | 8.21 | 0.1 | 0 | 0 | 0 | 0 | 0 | 0 | 0 | 0 | 0.01 | 0.82 | 9.14 |
| 2014 | 0.17 | 0.98 | 10.83 | 0.18 | 0.29 | 0 | 0 | 0 | 0 | 0.01 | 0.09 | 0.02 | 12.58 |
| 2015 | 0.19 | 1.5 | 0.07 | 0.01 | 0 | 0 | 0 | 0 | 0 | 1.14 | 0.26 | 0.61 | 3.8 |
| 2016 | 0.38 | 0.01 | 0.19 | 0 | 0 | 0 | 0 | 0 | 0.01 | 0.59 | 3.51 | 7.38 | 12.08 |
| 2017 | 0 | 0.04 | 0.15 | 4.2 | 0 | 0 | 0 | 0 | 0 | 0.09 | 2.19 | 0.06 | 6.73 |
| 2018 | 0.29 | 3.31 | 0.1 | 0.1 | 0.25 | 0 | 0 | 0 | 0.05 | 11.33 | 1.28 | 0.81 | 17.52 |
| 2019 | 0.07 | 2.65 | 0.75 | 0 | 0 | 0 | 0 | 0 | 0 | 0.08 | 0 | 6.34 | 9.89 |
| 2020 | 0.62 | 8.48 | 4.62 | 0.27 | 1.38 | 0 | 0 | 0 | 0 | 0.05 | 0.21 | 0.13 | 15.77 |

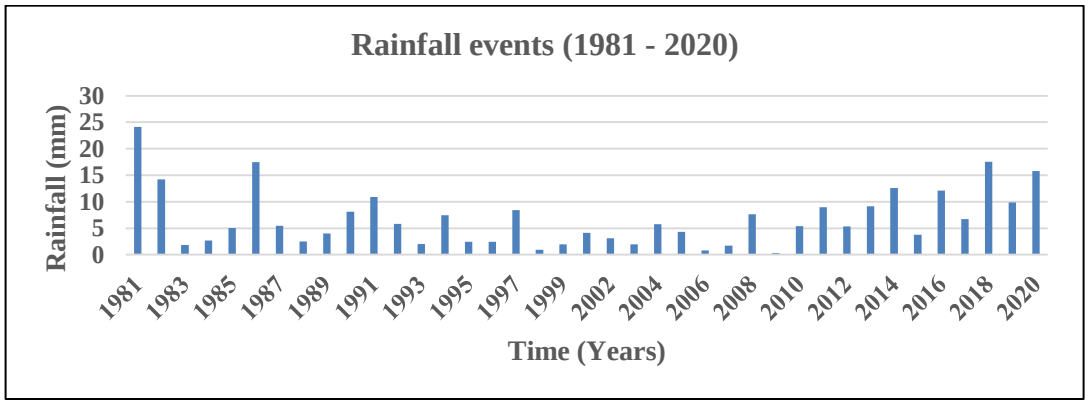


**Fig. (2): Annual average rainfall of the study area in the period from 1981 to 2020 (according to NASA POWER Project data, 2021).**

Multi-spectral remote sensing and geographic information systems (GIS) were integrated in order to optimize the surface water usage of episodic rainfalls, where the concept of runoff water harvesting (RWH) in promising watersheds should be applied. Runoff water harvesting is a tool that could provide the required water, which could be used for both domestic and agricultural development in arid lands (Elewa, et al., 2012; Elewa, et al., 2016; and Elewa, et al., 2020). The RS and GIS techniques had proved to be the most effective tools in performing the hydro-morphometric analysis and assessment.

Nowadays, RS and GIS techniques are used widely for determining and analyzing morphometric parameters of watersheds. Agarwal (1998), Nag (1998), and Das and Mukhrjee (2005) are the pioneer authors who used these techniques for such purpose. Morphometric analysis of a drainage basin demonstrates the dynamic equilibrium that has been achieved due to the interaction between matter and energy. Aher et al. (2014) used the geospatial–statistical techniques for identifying critical and potentiality sub-watersheds in water scarce areas, by applying weighted sum analysis technique for the morphometric parameters of the sub-watersheds. Javed et al. (2009) studied the prioritization of sub-watersheds based on morphometric and land use characteristics using remote sensing and GIS techniques. In this context, an attempt has been made to evaluate the RWH potentiality areas in El-Assiuti watershed using morphometric parameters as thematic layers or criteria for the weighted spatial probability modeling (WSPM). The performed model for El-Assiuti watershed was applied as a genuine approach through two different scenarios, involving equal weights to criteria, and weights justified by the sensitivity analysis. The sensitivity analysis in the present work was applied by the variance-based global sensitivity analysis (GSA) or what is called the analysis of variance (ANOVA) (Saisana et al. 2005).

Geologically, Wadi El-Assiuti is completely covered by sedimentary rocks belonging to different ages ranging from lower Eocene to Recent times (Fig. 3).

According to Said (1981 & 1990), and Conoco (1987), the lithostratigraphic units in descending order could be summarized as; **(1) Quaternary deposits** were described by many authors as: (a) Sand Sheet, Serir which are a surface of large, angular fragments. (b) Nile Silt which composed from silt, marl, and gravel interbeds. (c) Fanglomerates which are a conglomerate grains formed by lithification of alluvial fans. (d) Wadi deposits which consist mainly of sand-sized materials and cover all floors of wadis draining in the study area and they have had some relationship with the ancient Nile system (Said, 1990). (e) Neonile deposits which consist sediments of sands and gravels with clay and shale lenses. (f) Gravels which composed of very hard crystalline limestone, hard marly limestone, and partially recrystallized chalky limestone. **(2) Pliocene deposits**; consists of lacustrine limestone and marly limestone, white shale, interbedded

red-brown clays, thin fine-grained sand, silt laminae, flint pebbles, and conglomerate. **(3) The lower Eocene Sequence** is composed of limestone and dolomites that are represented by Maghagha, Minia, Drunka, and Serai /Thebes Formations.

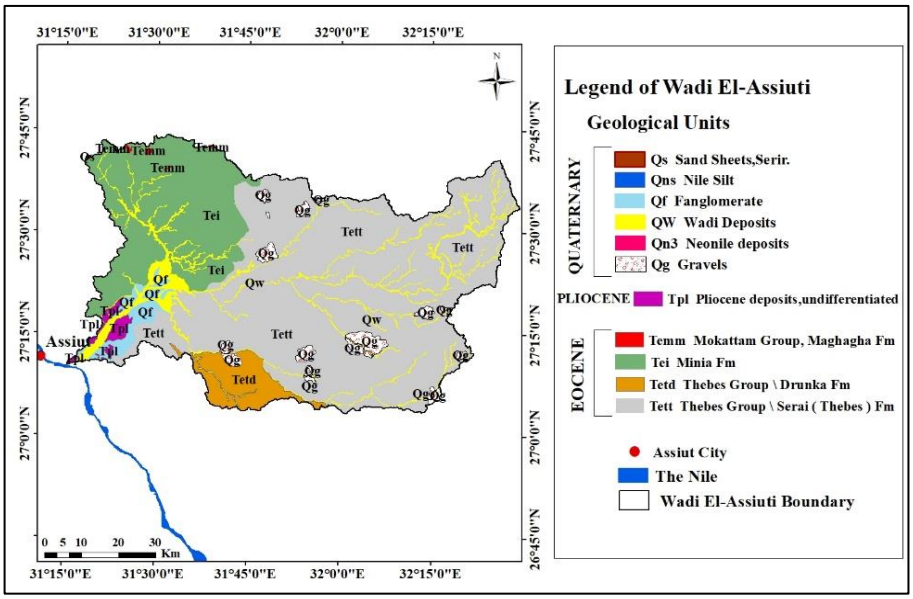


**Fig. (3): Geological map of Wadi El-Assiuti (modified after Conoco, 1987).**

Based on study given by Yousef (2008) on Wadi El-Assiuti, the main fault systems are NW (Clysmic), NE, and EW (Tethyan) in decreasing order (Fig. 4). The NW fault system had occurred in a later stage of faulting after the development of NE fault system where the NW fault system is relatively active. The exposed limestone around Wadi El-Assiuti area is highly dissected by major and minor joints (Omara and El-Tahlawi, 1972). The wadi slope varies from very gentle slopes (< 1 %) to moderately steep slopes (> 29 %) (Fig. 5), while the topography of the wadi ranges from < 230 (a.s.l.) m to rugged mountainous and hilly lands, and heights up to 620 m (a.s.l.) (Fig. 6).

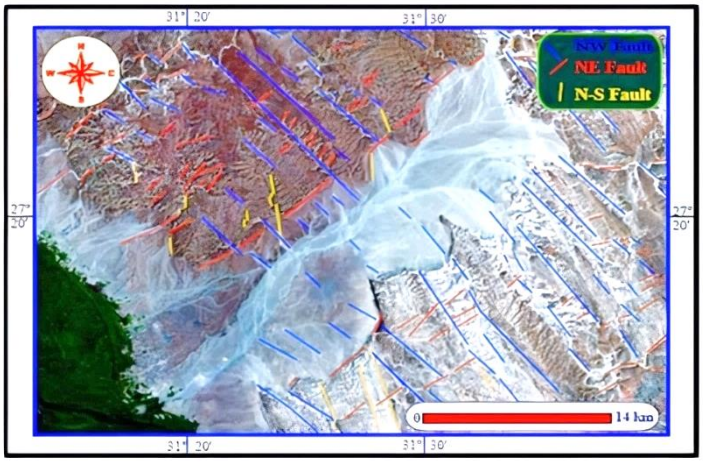


**Fig. (4): The main fault systems in Wadi El-Assiuti (after Yousef, 2008).**

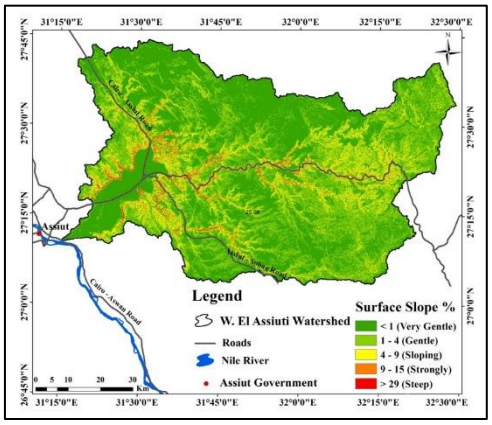


**Fig. (5): Slope map of study area (based on a 30-m resolution ASTER DEM).**

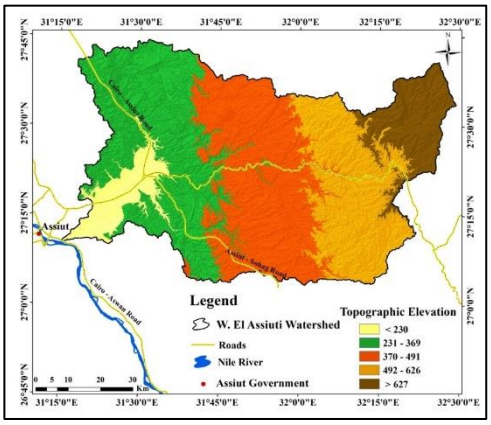


**Fig. (6: Topographic elevations of the study area (based on ASTER DEM of 30m resolution).**

## MATERIALS AND TECHNIQUES

The drainage net map of Wadi El-Assiuti watershed (Fig. 7) had been prepared using ASTER DEM with 30-m spatial resolution project on OLI+8 satellite image, which was verified with the information gained from topographic maps of 1:50,000 and 1:100,000 scales with the performed necessary ground truthing. Lithostratigraphic and soil data were collected from Conoco geological maps of the Eastern Desert (Conoco, 1987) of 1:500,000 scale. Processing and enhancement were performed on Landsat OLI+8 images using ERDAS Imagine 2015© software. The drainage pattern was constructed based on the ASTER DEM data using the WMS software 10.1©. The morphometric parameters of El-Assiuti sub-watersheds have been calculated using the ArcGIS 10.4 software. Perimeter and area of the sub-watersheds were also calculated by the ‘‘Measurement Tool’’ on the ASTER DEM data. The order was assigned to each stream by following Strahler stream ordering technique (Strahler 1964). The hydro-morphometric parameters of the study area basins’ watersheds were determined using Watershed Modeling Systems (WMS 10.1©) software (Aquaveo, 2018), which differentiates the basins and provides multiple watershed characteristics. The methods used to calculate the morphometric parameters are given in Table 2.

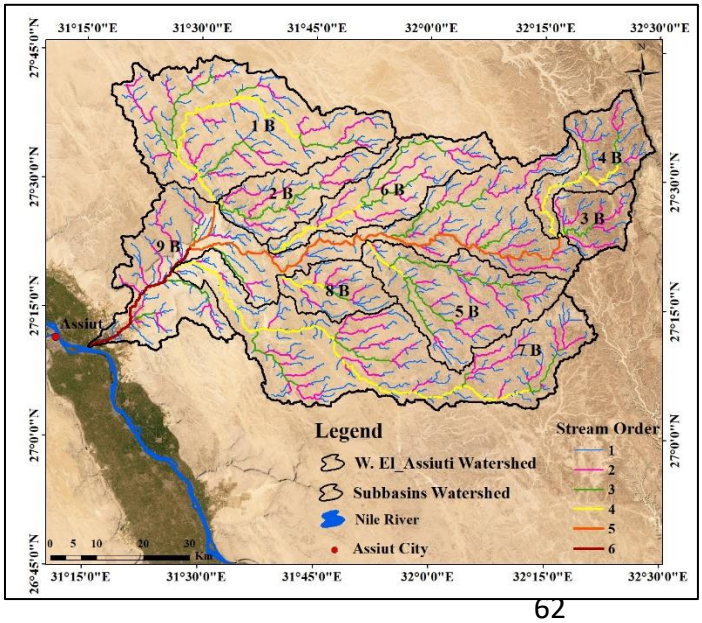


**Fig. (7): Satellite OLI+8 image showing Stream ordering and sub-watersheds of Wadi El-Assiuti.**

The WMS 10.1© software calculated the hydro-morphometric characteristics for each sub-watershed value used in the WSPM. These values are provided for each of the delineated watersheds. These layers are generated in steps, i.e., digitization, editing, building topological structure, and finally polygonization in the ArcGIS 10.4© Spatial Analyst module (ESRI, 2015).

**Table (2): Methods applied for the computation of morphometric parameters.**

| Aspect Type | Morphometric Parameter | Formula | Reference |
|---|---|---|---|
| Linear Aspects | Steam Order | Hierarchical Rank. | |
| | Bifurcation Ratio (Rb) | **Rb = Nu / Nu+1,** where, **Nu**= Number of stream segments present in the given order. **Nu+1**=Number of stream segments of the next higher order. | Schumn, 1956 |
| | Mean Bifurcation Ratio (Rbm) | **Rbm** = Average of Bifurcation Ratios of all orders. | Strahler, 1964 |
| | Stream Length (Lu) | Length of the Stream (km). | Horton, 1945 |
| | Mean Stream Length (Lsm) | **Lsm = Lu / Nu,** (km), where, **Lu** = Mean length of a given order (km). **Nu**= Number of stream segments. | Strahler, 1964 |
| | Stream Length Ratio (Rl) | **Rl = Lu / Lu-1,** where, Lu=Total stream length of order (u). **Lu-1**= The total stream length of its next lower order. | Horton, 1945 |
| Areal Aspects | Drainage Density (Dd) | **D = ∑Lu / Au,** (km/km$^2$), where, **Lu**= Total Stream of all orders (km). **Au**= Area of the Basin (km$^2$). | Horton, 1945 |
| | Drainage Texture (Rt) | **Rt = ∑Nu / P,** where, **Nu** = Stream number, **P** = Perimeter (km). | Horton, 1945 |
| | Stream Frequency (Fs) | **Fs = ∑ Nu / Au,** where, **Nu** = Total number of streams in the basin. **Au** = Basin Area (km$^2$). | Horton, 1945 |
| | Infiltration No. (If) | **If = Dd * Fs,** where, **Dd** = Drainage Density. **Fs** = Stream Frequency. | Faniran, 1968 |
| | Length of Over Land Flow (Lg) | **Lg = 1/ Dx2** (km), where, **D** = Drainage density (km/km$^2$). | Horton, 1945 |
| | Form Factor (Rf) | **Rf = Au / Lb$^2$,** where, **Au**= Basin area (km$^2$). **Lb** = Maximum basin length (km). | Horton, 1945 |
| | Circularity Ratio (Rc) | **Rc = 4πAu / P$^2$,** where, **Au** = Basin area (km$^2$). **P** = Premier of the basin (km) | Miller, 1953 |
| | Elongation Ratio (Re) | **Re= 2 $(\sqrt{Au/\pi})/Lb$,** where, **Au**= Area of the Basin (km$^2$). **Lb**= Maximum basin length (km). **π** = a constant equal 3.14 | Schumn, 1956 |
| Relief Aspects | Relief Ratio (Rh) | **Rh = H / Lb$_{max}$,** where, **H** = Maximum basin relief (km). **Lb$_{max}$**= Maximum basin length (km). | Schumn, 1956 |
| | Ruggedness No. (Rn) | **Rn = H * Dd** where, **H** = Maximum basin relief. **Dd** = Drainage density. | Strahler, 1964 |
| | Relative Relief (Rhp) | **Rhp = H * (100) / P,** where, **H** = Maximum basin relief. **P** = perimeter of the basin (km). | Melton, 1958 |

The WSPM for determining the RWH potentiality areas was performed using the eight thematic layers, basin area (BA), basin slope (BS), basin length (BL), drainage density (DD), maximum flow distance (MFD), length of overland flow (OFD), basin infiltration number (IF), and volume of annual flood (VAF) (calculated by SCS-CN method), inside the ArcGIS 10.4© software platform (Elewa, H. H. et al., 2021).

Runoff calculation model used is the Soil Conservation Service Curve Number (SCS-CN) (USDA SCS, 1989) method, which was run inside the WMS 10.1© software (Aquaveo, 2018). The purpose of using WMS is to calculate the peak flood discharge according to climate records in the sub-watersheds using digital elevation information and weighted curve numbers generated from the existing land use and soil data.

The prioritization process was achieved in the present work by applying the WSPM, which was developed through different scenarios with a detailed sensitivity analysis. The eight themes were converted into raster format and reclassified by the ‘‘Spatial Analyst’’ extension tool of the ArcGIS 10.4© software. Specific weights and ranks were assigned to each theme, while each individual layer class is based on its magnitude of contribution to the water holding capacity with respect to its relation to the other morphometric parameters (Javed et al., 2009).

Accordingly, the WSPM for the prioritization was performed by two different scenarios (Elewa, et al., 2018-2020): equal weights to criteria (scenario I) and weights justified by the sensitivity analysis (scenario II). The first scenario supposes that all the WSPM’s eight thematic layers have the same magnitude of contribution in the RWH priority mapping (equal weights of 12.5 %), while the second scenario is based on the sensitivity analysis techniques, which concentrate on the impact of individual morphometric parameters on the model output. In this scenario, a sensitivity analysis (Van Griensven et al. 2006) was performed to justify the weights of the WSPM’s criteria in order to attain a more justified or optimum RWH priority areas in El-Assiuti watershed. However, to justify the WSPM’s weights and results, we have to take all the scenarios as alternatives with different proposals for assigning the weights of criteria.

## RESULTS AND DISCUSSION

### 1 - Drainage morphometric analysis

The morphometric parameters of El-Assiuti watershed and its nine sub-watersheds (Fig. 7) had been determined and classified into linear and areal aspects. The linear aspects include: stream order, stream length, stream length ratio, mean stream length and bifurcation ratio, while the areal aspects include: drainage density, elongation ratio, circulatory ratio, drainage texture, stream frequency, form factor and length of the overland flow (Table 2). The development of surface drainage networks and their actions were described according to the basics of quantitative physiographic methods (Leopold and Maddock, 1953).

### 1.1- Stream ordering

The description of stream orders is the first step in watershed quantitative analysis. It is based on the hierarchical relationship between stream segments (Table 2). It had been observed that the total El-Assiuti watershed have streams up to the $6^{th}$ order (Fig. 7). Eight sub-watersheds have streams ranked up to the $4^{th}$ order, with the exception of the Center El-Assiuti sub-watershed, which have streams that exceed to the $5^{th}$ order (Table 3).

**Table (3): Results of morphometric analysis of watershed linear aspects of Wadi El-Assiuti watershed (Lu, $L_{sm}$, and $R_l$).**

| Stream order | Sub-Basin B1 | | | | | Sub-Basin B2 | | | | | Sub-Basin B3 | | | | |
|---|---|---|---|---|---|---|---|---|---|---|---|---|---|---|---|
| | Stream no. | Bifurcation ratio (Rb) | Stream length ($L_u$) (km) | Mean stream ($L_{sm}$) (km) | Stream length ratio ($R_l$) | Stream no. | Bifurcation ratio (Rb) | Stream length ($L_u$) (km) | Mean stream ($L_{sm}$) (km) | Stream length ratio ($R_l$) | Stream no. | Bifurcation ratio (Rb) | Stream length ($L_u$) (km) | Mean stream ($L_{sm}$) (km) | Stream length ratio ($R_l$) |
| 1st | 119 | 4.25 | 244.79 | 2.06 | 0.57 | 32 | 4.57 | 88.65 | 2.77 | 0.65 | 23 | 3.83 | 39.25 | 1.71 | 1.29 |
| 2nd | 28 | 3.50 | 140.23 | 5.01 | 0.57 | 7 | 3.50 | 58.03 | 8.289 | 0.59 | 6 | 3.00 | 50.76 | 8.46 | 0.29 |
| 3rd | 8 | 8.00 | 79.41 | 9.93 | 0.77 | 2 | 2.00 | 34.40 | 17.20 | 0.04 | 2 | 2.00 | 14.97 | 7.48 | 0.06 |
| 4th | 1 | | 61.68 | 61.68 | | 1 | | 1.22 | 1.22 | | 1 | | 0.97 | 0.97 | |
| Stream order | Sub-Basin B4 | | | | | Sub-Basin B5 | | | | | Sub-Basin B6 | | | | |
| | Stream no. | Bifurcation ratio (Rb) | Stream length ($L_u$) (km) | Mean stream ($L_{sm}$) (km) | Stream length ratio ($R_l$) | Stream no. | Bifurcation ratio (Rb) | Stream length ($L_u$) (km) | Mean stream ($L_{sm}$) (km) | Stream length ratio ($R_l$) | Stream no. | Bifurcation ratio (Rb) | Stream length ($L_u$) (km) | Mean stream ($L_{sm}$) (km) | Stream length ratio ($R_l$) |
| 1st | 36 | 4.00 | 77.37 | 2.15 | 0.44 | 76 | 5.43 | 149.43 | 1.96 | 0.49 | 44 | 4.00 | 92.38 | 2.09 | 0.71 |
| 2nd | 9 | 3.00 | 34.10 | 3.79 | 0.62 | 14 | 4.67 | 74.60 | 5.33 | 0.96 | 11 | 5.50 | 65.94 | 5.99 | 0.74 |
| 3rd | 3 | 3.00 | 21.07 | 7.03 | 1.74 | 3 | 3.00 | 71.37 | 23.79 | 0.18 | 2 | 2.00 | 49.03 | 24.51 | 0.56 |
| 4th | 1 | | 36.70 | 36.70 | 0.44 | 1 | | 13.03 | 13.03 | | 1 | | 27.48 | 27.48 | |
| Stream order | Sub-Basin B7 | | | | | Sub-Basin B8 | | | | | Sub-Basin B9 | | | | |
| | Stream no. | Bifurcation ratio (Rb) | Stream length ($L_u$) (km) | Mean stream ($L_{sm}$) (km) | Stream length ratio ($R_l$) | Stream no. | Bifurcation ratio (Rb) | Stream length ($L_u$) (km) | Mean stream ($L_{sm}$) (km) | Stream length ratio ($R_l$) | Stream no. | Bifurcation ratio (Rb) | Stream length ($L_u$) (km) | Mean stream ($L_{sm}$) (km) | Stream length ratio ($R_l$) |
| 1st | 132 | 4.26 | 301.82 | 2.28 | 0.59 | 23 | 3.28 | 72.50 | 3.152 | 0.41 | 157 | 4.76 | 355.13 | 2.26 | 0.89 |
| 2nd | 31 | 5.17 | 180.46 | 5.82 | 0.33 | 7 | 3.50 | 29.78 | 4.25 | 0.28 | 33 | 4.13 | 316.82 | 9.60 | 10.25 |
| 3rd | 6 | 6.00 | 59.76 | 9.96 | 1.77 | 2 | 2.00 | 8.52 | 4.26 | 1.44 | 8 | 4.00 | 3246.15 | 405.77 | 0.04 |
| 4th | 1 | | 105.81 | 105.81 | | 1 | | 12.29 | 12.29 | | 2 | 2.00 | 122.75 | 61.37 | 0.30 |
| 5th | | | | | | | | | | | 1 | | 37.28 | 37.28 | |

### 1.2- Stream length (Lu)

It was observed that the maximum total length of stream segments represents the first order (Table 3). It is also observed that the stream length values decreased as the stream order increased in sub-watersheds (B1, B2, B5, and B6) while in the other sub-watersheds of Wadi El-Assiuti, the stream length is changing between the stream orders.

### 1.3 -Mean stream length ($L_{sm}$)

In the study area, the values of $L_{sm}$ for all orders in Wadi El-Assiuti sub-watersheds vary from 0.97 km in the B3 sub-watershed to 405.77 km in the B9 sub-watershed (Table 3). In sub-

watersheds (B4, B7, and B8), the value of $L_{sm}$ of any given order is lower than that of the next higher-order, while in the other sub-watersheds of the wadi, the values of $L_{sm}$ show an irregularity between the different stream orders.

### 1.4 - Bifurcation ratio (Rb)

It is observed that the Rb values in most of Wadi El-Assiuti sub-watersheds are between 2.0 and 5.0, which indicate that the geological structures do not deform the drainage pattern (Strahler, 1964). There are some Rb values out of this range, which appear for 3rd stream orders in B1 and B7 sub-watersheds. Mean Rb values are varied between 2.00 for B1, B3, B6, B8, and B9 sub-watersheds and 5.50 for B6 sub-watershed (Table 3).

### 1.5 - Stream length ratio ($R_l$)

Stream length ratio values of Wadi El-Assiuti sub-watersheds show an increase from the lower order to the next higher-order in sub-watersheds of B1 and B4. In B2 and B3 sub-watersheds, $R_l$ values decreased from one order to the next higher order. In the other sub-watersheds of Wadi El-Assiuti, there are irregularities between the stream orders (Table 3).

### 1.6 - Drainage density (DD)

The DD values of Wadi El-Assiuti sub-watersheds varied from 0.48 $km^{-1}$ in B1 sub-watershed to 2.75 $km^{-1}$ in B9 sub-watershed (Table 4). Nag (1998) suggested that moderate DD indicates that the basin has moderately permeable sub-soil and thick vegetative cover. The higher DD values in Wadi El-Assiuti were observed in B9, B8, and B6 sub-watersheds, which designate high flooding RWH possibilities.

### 1.7 - -Drainage texture (DT)

DT values were classified by Smith (1950) into five different textures: i.e. (< 2) for very coarse, (2 to 4) for course, (4 to 6) for moderate, (6 to 8) for fine, and (> 8) for the very fine texture. The DT of all the Wadi El-Assiuti sub-watersheds is falling in the category of very coarse texture. The DT values vary from 0.28 in B2 sub-watershed to 0.64 in B1 sub-watershed (Table 4).

**Table (4): Morphometric analysis of areal aspects of Wadi El-Assiuti sub-watersheds.**

| Sub-Basin | Drainage density (DD) | Drainage texture (DT) | Stream frequency (FS) | Infiltration number (IF) | Form factor (FF) | Circularity ratio (RC) | Elongation ratio (RE) | Length of overland flow (LG) |
|---|---|---|---|---|---|---|---|---|
| B1 | 0.48 | 0.64 | 0.14 | 0.07 | 0.62 | 0.23 | 0.44 | 0.24 |
| B2 | 0.54 | 0.28 | 0.13 | 0.07 | 0.19 | 0.19 | 0.25 | 0.27 |
| B3 | 0.54 | 0.38 | 0.16 | 0.09 | 0.56 | 0.36 | 0.42 | 0.27 |
| B4 | 0.49 | 0.33 | 0.14 | 0.07 | 0.28 | 0.19 | 0.29 | 0.25 |
| B5 | 0.49 | 0.52 | 0.15 | 0.07 | 0.32 | 0.24 | 0.32 | 0.25 |
| B6 | 0.52 | 0.32 | 0.13 | 0.07 | 0.16 | 0.17 | 0.22 | 0.26 |
| B7 | 0.51 | 0.46 | 0.13 | 0.07 | 0.15 | 0.12 | 0.22 | 0.25 |
| B8 | 0.55 | 0.33 | 0.15 | 0.08 | 0.34 | 0.28 | 0.33 | 0.27 |
| B9 | 2.75 | 0.36 | 0.14 | 0.37 | 0.12 | 0.06 | 0.19 | 1.37 |

### 1.8 - Stream frequency (FS)

The greater the DD and FS in a basin, the greater the runoff velocity, the more hazards they may cause, and the more need for conducting RWH techniques (Elewa et al., 2014). The highest FS value was observed in B3 sub-watershed, which has a relatively high DD value (Table 4).

### 1.9 -Infiltration number (IF)

The IF of Wadi El-Assiuti sub-watersheds varies between 0.07 in B1, B2, B4, B5, B6 and B7 sub-watersheds and 0.37 in B9 sub-watershed, which also has the highest DD (2.75 $km^{-1}$) (Table 4). IF values of Wadi El-Assiuti sub-watersheds are low and close to each other with an average value of 0.11 which indicate high infiltration rate, consequently high groundwater recharge possibilities by rain water harvesting.

### 1.10- Form factor (FF)

The form factor value should be always less than 0.7854 (the value corresponding to a perfectly circular basin). The calculated values of FF varied from 0.12 in B9 sub-watershed to 0.62 in B1 sub-watershed (Table 4). FF values are relatively low for most of Wadi El-Assiuti sub-watersheds reflecting the more or less elongated shape of the basins.

### 1.11 - Circulatory ratio (RC)

Horton (1945) gave values of the circulatory ratios of 0.6 to 0.7 in homogenous geological materials to preserve their geometric symmetry. The RC values of Wadi El-Assiuti sub-watersheds are generally low with an average value of 0.21, while the lowest RC value was observed in B9 sub-watershed (Table 4).

### 1.12 - Elongation ratio (RE)

Strahler (1964) proposed a classification for the elongation ratio as the following: (< 0.7) for the less elongated, (0.8-0.9) for the oval, (> 0.9) for the circular basins. The values nearby to 1.0 are typical for the regions of very low relief, whereas the values between 0.6 and 0.8 are generally associated with strong relief and steep ground slope. The values of RE for Wadi El-Assiuti sub-watersheds range between 0.19 and 0.44 (Table 4).

### 1.13 - Length of overland flow (LG)

The lowest value of LG (0.24 km) was recorded in B1 sub-watershed reflecting the shortest length of overland flow, and consequently the quickest runoff process. The highest LG value was observed in B9 (1.37 km) indicating the longer length of overland flow and a slow runoff process (Table 4).

### 1.14- Relief ratio (RH)

The higher the RH, the higher the slope of the basin, and the lower the IF and the higher the runoff flow velocity. The values of RH of Wadi El-Assiuti sub-watersheds range between 0.58 in B7 sub-watershed and 1.08 in B3 sub-watershed. These relief ratios reflect the flat to steep slopes through the sub-watersheds of the wadi (Table 5).

**Table (5): Morphometric analysis of relief aspects of Wadi El-Assiuti sub-watersheds.**

| Sub-Basin Name | Relief Ratio (RH) | Ruggedness Number (RN) |
|---|---|---|
| **B1** | 0.68 | 0.14 |
| **B2** | 0.69 | 0.16 |
| **B3** | 1.08 | 0.11 |
| **B4** | 0.91 | 0.16 |
| **B5** | 0.73 | 0.16 |
| **B6** | 0.76 | 0.21 |
| **B7** | 0.58 | 0.27 |
| **B8** | 0.88 | 0.12 |
| **B9** | 0.61 | 1.88 |

### 1.15 - Ruggedness number (RN)

The calculated values of RN are variable between 0.11 in B3 sub-watershed and 1.88 in B9 sub-watershed (Table 5). The variation in RN values reflects the difference in slope and relief between the sub-watersheds of Wadi El-Assiuti watershed.

### 2 - Prioritization of El-Assiuti sub-watersheds for runoff water harvesting

The multi-criteria decision support layers are to be translated into data coverage after establishing the watershed characteristics using the DEMs inside the platform of WMS 10.1© software for simpler data storage and manipulation. The input criteria (layers) and their ranges used in the construction of the WSPM include; volume of annual flood (VAF), basin slope (BS), drainage density (DD), maximum flow distance (MFD), overland flow distance (OFD), basin area (BA), basin length (BL) and basin infiltration number (IF). When these criteria are included into the GIS-based WSPM, detailed maps identifying effective sites suitable for RWH with various classes will be produced. Detailed description of Wadi El-Assiuti watershed is given hereinunder.

### 2.1 - Hydro-morphometric parameters of Wadi El-Assiuti

The area of Wadi El-Assiuti is an important parameter in basin analysis, and it is delineated by the water divide. In the present work, basin area was calculated using the ArcGIS 10.4© Software (Table 6). The total area of Wadi El-Assiuti is ~6018 $km^2$. Basin perimeter is the outer boundary of the watershed that enclosed its area (Kuldeep and Upasana, 2001). Basin perimeter of Wadi El-Assiuti is ~ 640 km. Basin relief of the watersheds plays an important role in drainage development, surface and subsurface water flow, permeability, landforms development and erosion properties of the terrain (Obi Reddy et al., 2002). Basin relief of Wadi El-Assiuti is 0.64 km (Table 6). Wadi El-Assiuti is characterized by relatively high value of drainage density 0.51 $km^{-1}$ that designate to high flooding RWH possibilities. Basin infiltration number of Wadi El-Assiuti is low 0.07, which indicates high potentiality for groundwater recharge by flash flood water.

**Table (6): Hydrographical output parameters from WMS of Wadi El-Assiuti basin.**

| Basin area BA ($km^2$) | Basin perimeter BP (km) | Drainage density DD ($km^{-1}$) | Stream frequency FS ($km^{-2}$) | Infiltration number IF |
|---|---|---|---|---|
| 6018.2 | 640.05 | 0.51 | 0.136 | 0.07 |
| **Ruggedness number RN** | **Basin relief BR (km)** | **Circularity ratio RC** | **Elongation ratio RE** | **Length of overland flow LG (km)** |
| 0.42 | 0.64 | 0.185 | 0.341 | 0.257 |

### 2.2 - Criteria of RWH potentiality determination in Wadi El-Assiuti watershed

By spatially integrating eight thematic layers, the RWH potentiality thematic layers of the Wadi El-Assiuti watershed were identified. The following is a short description of these themes (Table 6):

**1- Average overland flow distance (OFD)**

The rainfall is called surface runoff when it reaches the channels (Horton, 1945). Most parts of Wadi El-Assiuti are represented by very low OFD classes. Low OFD class is represented by some parts of the eastern side of the Wadi (Fig. 8-A).

**2- Volume of annual flood (VAF)**

The VAF reflects the quantity of water available for harvesting. The VAF was calculated by SCS-CN method (USDA SCS, 1989) (Table 7). According to the VAF map, the larger area of Wadi El-Assiuti is occupied by moderate VAF class (1,309,300 – 1,704,200 $m^3$). High to very high classes occur as small zones on the northwestern parts of the Wadi, where very low class occupied by small parts of the Wadi (Fig. 8-B).

**3- Basin slope (BS)**

High and very high BS classes are occupied by small parts of the northeastern side of Wadi El-Assiuti, while moderate BS class (0.0488 – 0.0522 m/m) is represented by most parts of eastern side (Fig. 8-C). The BS decreases towards of the western side of Wadi El-Assiuti until it reaches to very low slope (< 0.0432 m/m) at the northwestern corner of the wadi.

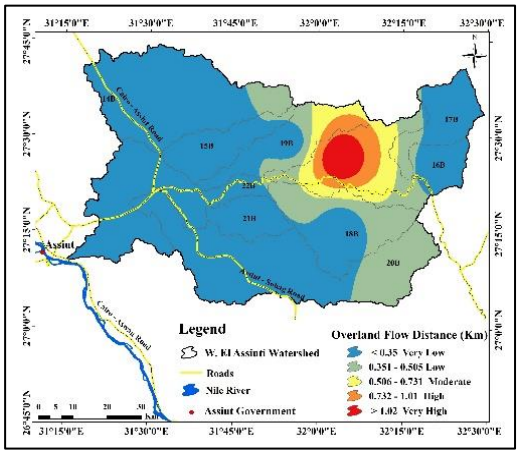


**(A)** The **OFD** thematic layer

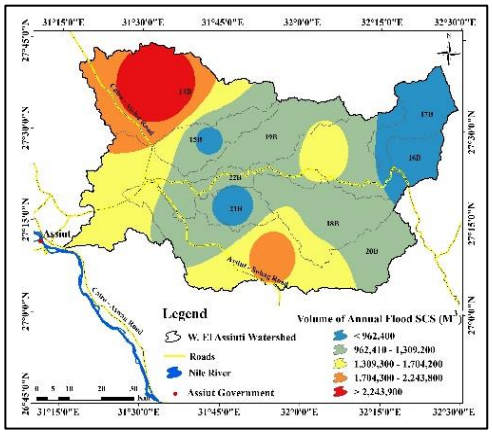


**(B)** The **VAF** thematic layer

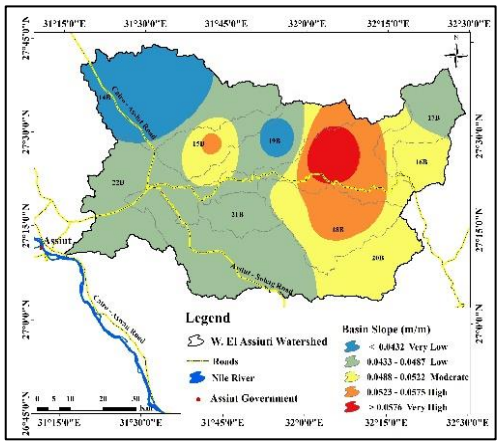


**(C)** The **BS** thematic layer

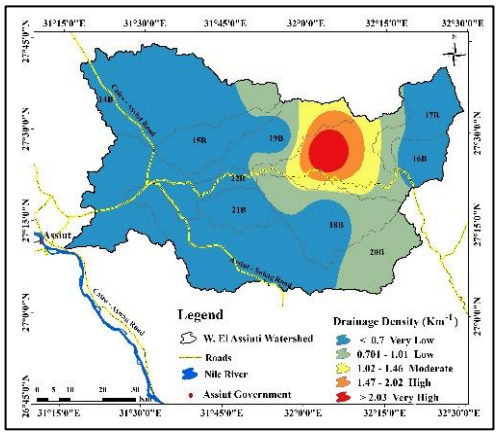


**(D)** The **DD** thematic layer

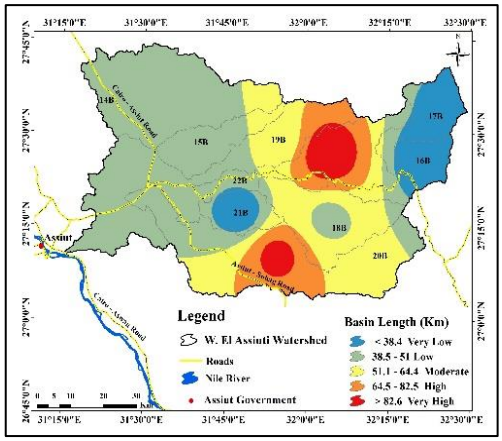


**(E)** The **BL** thematic layer

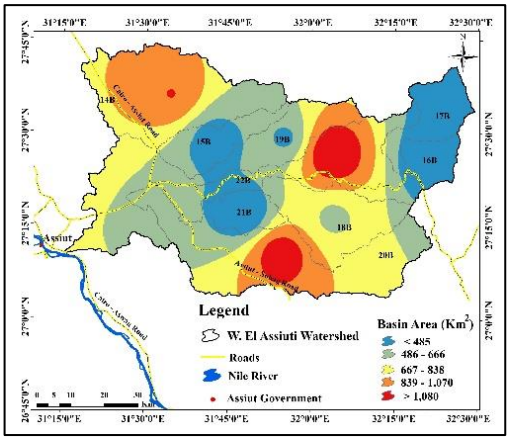


**(F)** The **BA** thematic layer

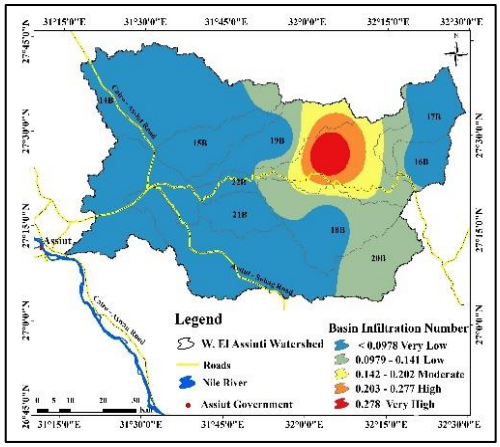


**(G)** The **IF** thematic layer

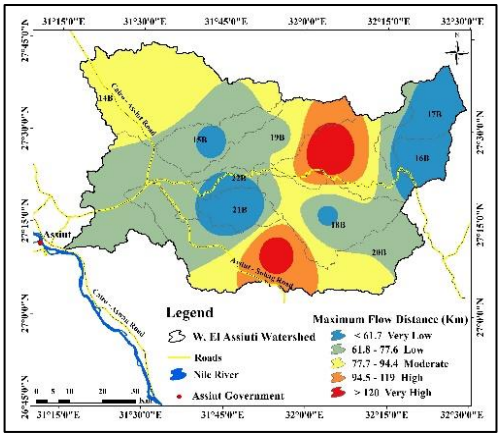


**(H)** The **MFD** thematic layer

**Fig. (8): The thematic layers which used in the WSPM of Wadi El-Assiuti watershed.**

**Table (7) Ranges of input criteria used in the WSPM for Wadi El-Assiuti watershed.**

| Watershed RWH Criteria | Very low | Low | Moderate | High | Very high |
|---|---|---|---|---|---|
| Volume of annual flood calculated by SCS-CN method ($m^3$) | < 962,400 | 962,410 - 1,309,200 | 1,309,300 - 1,704,200 | 1,704,300 - 2,243,800 | > 2,243,900 |
| Overland flow distance (km) | < 0.35 | 0.351 - 0.505 | 0.506 - 0.731 | 0.732 - 1.01 | > 1.02 |
| Maximum flow distance (m) | < 61.7 | 61.8 - 77.6 | 77.7 - 94.4 | 94.5- 119 | > 120 |
| Basin infiltration number | < 0.0978 | 0.0979 - 0.141 | 0.142 - 0.202 | 0.203 - 0.277 | > 0.278 |
| Drainage density ($km^{-1}$) | < 0.7 | 0.701 - 1.01 | 1.02 - 1.46 | 1.47 - 2.02 | > 2.03 |
| Basin area ($km^2$) | < 485 | 486 – 666 | 667 - 838 | 839 - 1,070 | > 1,080 |
| Basin slope (m/m) | < 0.0432 | 0.0433 - 0.0487 | 0.0488 - 0.0522 | 0.0523 - 0.0575 | > 0.0576 |
| Basin length (km) | < 38.4 | 38.5 – 51 | 51.1 - 64.4 | 64.5 - 82.5 | > 82.6 |

## 4- Drainage density (DD)

The higher the DD the higher is the RWH potential, and vice versa. Most parts of Wadi El-Assiuti are represented by very low DD class (< 0.7 $km^{-1}$) especially in the central and western parts (Fig. 8-D). High, very high and moderate DD classes are occupied by small parts of the northeastern side of the wadi.

## 5- Basin length (BL)

The longer the BL, the lower the chances that such a basin will be flooded. This is because the longer the basin, the lower its slope and hence the higher the possibilities for the RWH. Very

high BL class is represented by the northeastern corner of Wadi El-Assiuti watershed in addition to small zone in the central part (Fig. 8-E).

**6- Basin area (BA)**

Basin area is the most important morphometric parameters that control the catchment runoff volume and pattern. The very high to high basin area classes (>839 $km^2$) occur as small zones in the southern and northeastern parts of Wadi El-Assiuti (Fig. 8-F).

**7- Basin infiltration number (IF)**

The higher the infiltration number the lower will be the infiltration and consequently, higher will be the runoff. Most parts of the wadi are represented by very low IF class, indicating high infiltration capacity and high chance for groundwater recharge by runoff water (Fig. 8-G).

**8- Maximum flow distance (MFD)**

This factor is important in determining the RWH capability of a drainage basin, as the higher the MFD, the higher the RWH possibilities, and vice versa. The very high and high MFD classes occur as two small zones in the northeastern and southeastern parts of the wadi (Fig. 8-H).

## RUNOFF WATER HARVESTING (RWH) MODEL RESULTS

The thematic layers used for the model construction have different measuring units and values. So, to remedy the problem of integration of these layers, each thematic layer values were normalized to the same values, ranged from 1 to 10.

In the first WSPM scenario (scenario I) (equal weights to criteria) assumes that the weights and rates of the previously discussed criteria are having equal weights of contribution in the RWH potentiality mapping (Table 8), where the integrated criteria were given an equal weight of 12.5 % with a summation of 100 % for all data themes. The classes were graded from I (very high potentiality) up to V (very low potentiality) (Table 8; Fig. 9). The degree of effectiveness (E) for each thematic layer was calculated by multiplying the criterion weight ($W_c$) with the criterion rank ($R_c$) (Eq. 1).

$$E = W_c \times R_c = 0.125 \times 90 = 11.25 \quad \text{[Eq.1]}$$

According to this method of data manipulation, the assessment of the effectiveness of each decision criterion provides a comparative analysis among the different thematic layers.

**Table (8): WSPM scenario I (equal weights to criteria), ranks and degree of effectiveness of themes used in the RWH potentiality mapping of Wadi El-Assiuti watershed.**

| Thematic layer (Criterion) | RWH potentiality class | Average rate (Rank) (Rc) | Weight (Wc) | Degree of effectiveness (E) |
|---|---|---|---|---|
| VAF, OFD, MFD, IF, DD, BA, BS, and BL. | I (Very high) | 0.9 | 12.5 | 11.25 |
| | II (High) | 0.7 | | 8.75 |
| | III (Moderate) | 0.5 | | 6.25 |
| | IV (Low) | 0.3 | | 3.75 |
| | V (Very low) | 0.1 | | 1.25 |

Thus, the WSPM output maps for the RWH potentiality with five classes ranging from very low to very high potentiality were produced (Fig. 9). The percentages of the spatial distribution of the resulting RWH potentiality classes to the total study area of Wadi El-Assiuti are given in table 9 for the RWH potentiality map constructed using the VAF which was calculated by

the USDA-SCS-CN method (Fig. 9). The distribution of the RWH potentiality classes, whereas high, very high, and moderate RWH classes are occupied by small zone in the northeastern part of the watershed, while low and very low RWH classes are represented by the eastern and western sides of the watershed (Fig. 9).

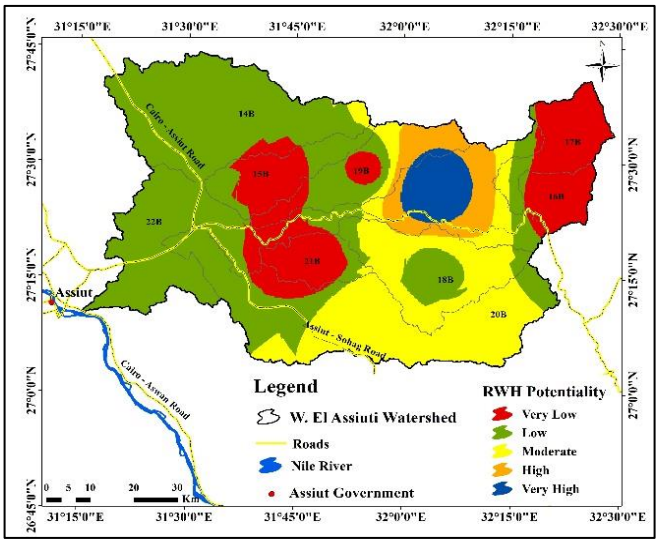


**Fig. (9): WSPM's scenario I map showing the potential areas for the RWH of Wadi El-Assiuti watershed.**

**Table (9): Areas of RWH potentiality classes for Wadi El-Assiuti watershed (WSPM Scenario I).**

| RWH Potentiality Class | Very low | Low | Moderate | High | Very high |
|---|---|---|---|---|---|
| Area ($km^2$) | 1172.05 | 2853.92 | 1404.26 | 353.54 | 232.89 |
| Area (in % relative to the total watershed area) (Total study area: 6016.67 $km^2$) | 19.48 | 47.43 | 23.34 | 5.88 | 3.87 |

The second scenario was to determine the RWH potentiality by applying the sensitivity analysis to justify the weights of the decisive criteria. In each WSPM's running operation, seven parameters had been kept with equal weights of 10 %, while assigning only one parameter with the remaining 30 % (Fig. 10). The previously discussed WSPM's running practice is necessary to apply the variance-based global sensitivity analysis (GSA), which subdivides the variability and apportions it to the uncertain inputs (Ha et al. 2012; Feizizadeh et al. 2004). GSA is based on perturbations of the entire parameter space, where input factors are examined both individually and in combination (Ligmann- Zielinska 2013). Variance-based GSA has been used in the present work. The goal of variance-based GSA is to quantitatively determine the weights that have the most influence on the model output, in this instance on the RWH categorization computed for each cell of the watershed area by the decisive factors.

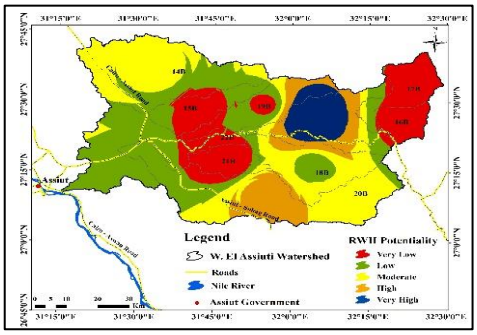


**BA 30 %**

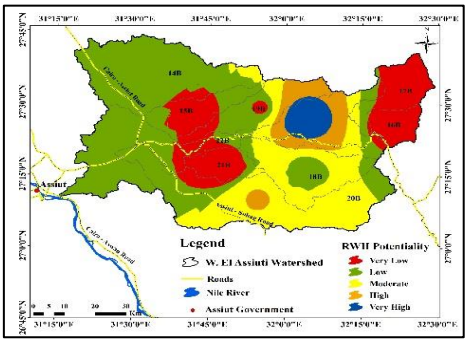


**BL 30 %**

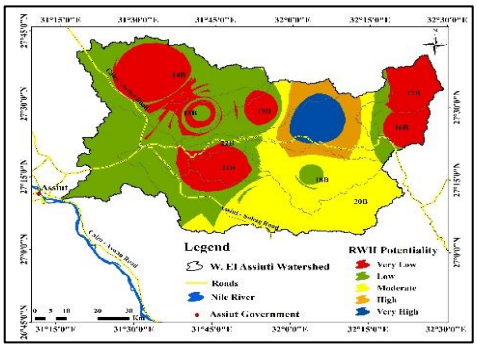


**BS 30 %**

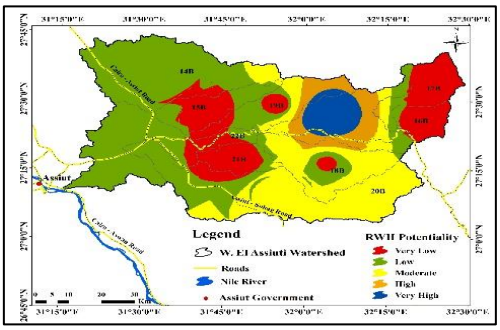


**DD 30 %**

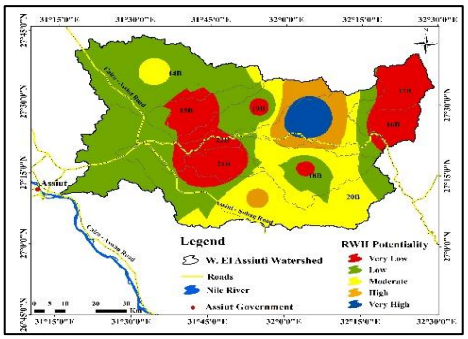


**MFD 30 %**

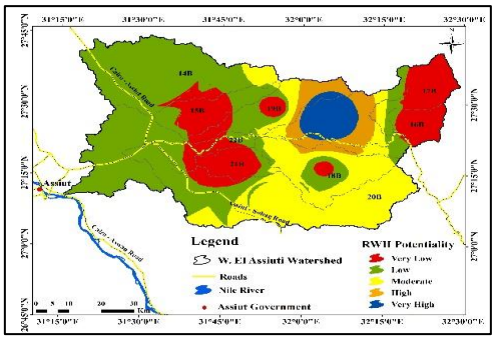


**OFD 30 %**

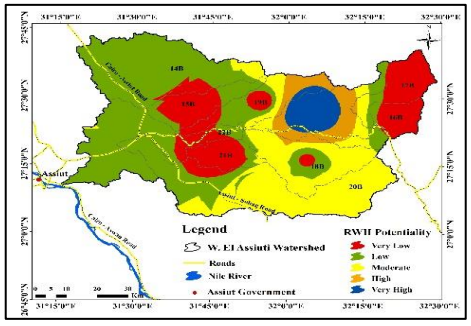


**IF 30 %**

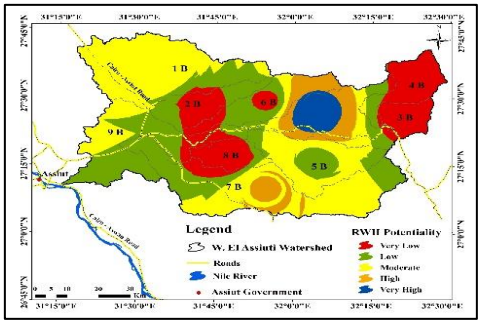


**FAV (SCS-CN) 30 %**

**Fig. (10): WSPM maps showing the potential areas for the RWH in Wadi El-Assiuti watershed (unequal weights: 10% for each thematic layer except one layer 30%).**

The importance of a given input factor (*Xi*) can be measured via the so-called sensitivity index, which is defined as the fractional contribution to the model output variance due to the uncertainty in (*Xi*). For (*k*) independent input factors, the sensitivity indices can be computed using the following decomposition formula for the total output variance [*V(Y)*] of the output (*Y*) (Saisana et al., 2005) (Eqs. 2–4):

$$V(Y)=\sum_{i} V_i + \sum_{i}\sum_{j>i} V_{ij} + \cdots + V_{12..k} \qquad \text{[Eq. 2]}$$

$$V_i = V_{xi}\left\{E_{x-i}\left(\frac{Y}{X_i}\right)\right\} \qquad \text{[Eq. 3]}$$

$$V_{ij} = V_{xixj}\left\{E_{x-ij}\left(\frac{Y}{X_i}, X_j\right)\right\} - V_{xi}\left\{E_{x-i}\left(\frac{Y}{X_i}\right)\right\} - V_{xj}\left\{E_{x-j}\left(\frac{Y}{X_j}\right)\right\} \qquad \text{[Eq. 4]}$$

A partial variance ($V_i$) represents the repeated variation of a single criterion (*i*), one of the eight model criteria that affects the other model criteria, which constitutes the inputs of the WSPM. In other words, one of the WSPM eight parameters is changed while the others remain constant. However, in Eq. 4, higher-order effects (*V1, 2 …p*) are combined effects for two or more inputs.

Figure 11 shows the classes of the high - very high RWH potentiality and their summation area (blue columns), which resulted from scenario I (equal weighting) and the scenario II, in which all criteria have equal weights of 10% except only one criterion with a weight of 30% for the wadi.

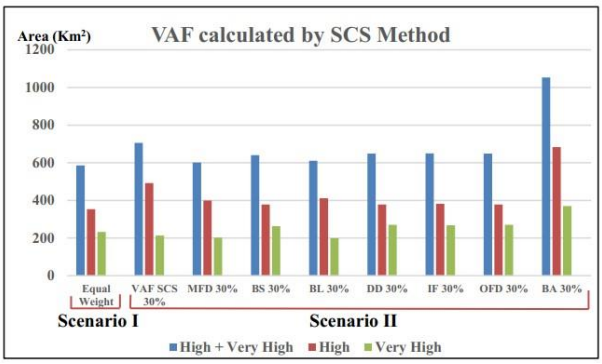


**Fig. (11) Areas (in km$^2$) of the High-Very high RWH potentiality classes and their summation in the two WSPM scenarios for Wadi El-Assiuti.**

Consequently, Figure 12 represents the percentage of variance in the total area of high and very high potentiality classes for the RWH, which had been resulted from scenario II comparable to scenario I which constructed by using VAF calculated by SCS-CN method. So, it could be noticed that the BA and VAF-SCS have the higher effect values. From Fig. 12 and Table 10, the summation of all variance ratios in the high - very high RWH potentiality classes in scenario II for each criterion with respect to their areas in scenario I is 148.01%. Accordingly, the justified weight of each criterion was calculated by dividing the variance ratio shown in by the total of all variance ratios Fig. 12 and Table 10.

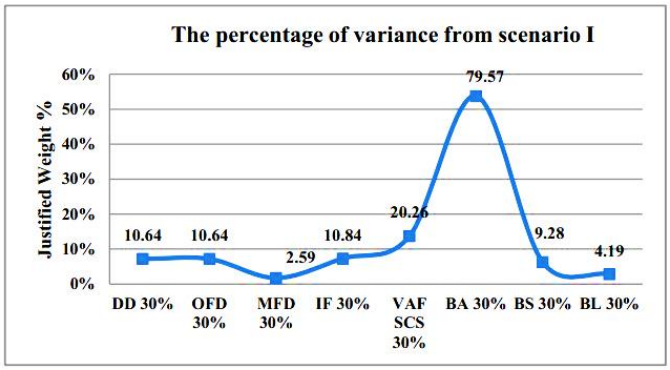


**Fig. (12): A graph indicating the variance ratios of the High-Very High classes in scenario II with respect to their areas in scenario I of Wadi El-Assiuti.**

**Table (10): The variance ratios and justified weights of the WSPM's criteria used in the RWH potentiality mapping of Wadi El-Assiuti watershed.**

| WSPM Criterion | DD 30% | OFD 30% | MFD 30% | IF 30% | VAF SCS 30% | BA 30% | BS 30% | BL 30% |
|---|---|---|---|---|---|---|---|---|
| Variance ratio % | 10.64 | 10.64 | 2.59 | 10.83 | 20.25 | 79.57 | 9.28 | 4.19 |
| Justified weight % | 7.19 | 7.19 | 1.75 | 7.32 | 13.68 | 53.76 | 6.27 | 2.84 |

Depending on the justified or optimum weights of thematic layers, another run of the WSPM was carried out taking into consideration these new weights of the used parameters (Table 10). The WSPM output map with five RWH potentiality classes ranging from the very low to very high were obtained (Fig. 13). The spatial distribution of these classes relative to the total study area was given Table 11.

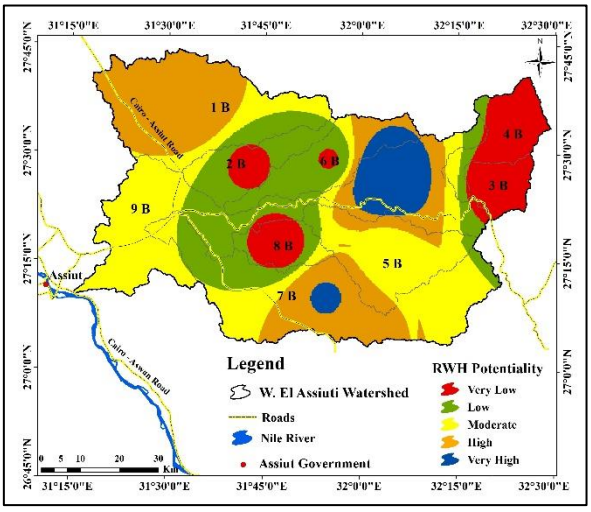


**Fig. (13) WSPM map (Based on sensitivity results) showing the potential areas for RWH in Wadi El-Assiuti watershed.**

**Table (11): Areas of RWH potentiality classes in Wadi El-Assiuti watershed (WSPM Scenario II; based on the results of sensitivity analysis).**

| RWH Potentiality Class | Very low | Low | Moderate | High | Very high |
|---|---|---|---|---|---|
| Area ($km^2$) | 1149.94 | 1860.83 | 2300.74 | 491.77 | 213.39 |
| Area (in % relative to the total watershed area) (Total study area: 6016.67 $km^2$) | 19.11% | 30.93% | 38.24% | 8.17% | 3.55% |

In conclusion, the WSPM's maps of scenario II, which had been constructed by the justified weights, were compared with scenario I, and with the field verification carried out by the research team. Accordingly, the justified scenario II could be considered as a product of high

reliability for determining the RWH potentiality, where it also coincides with the local inhabitants' experience and needs.

## CONCLUSION

Wadi El-Assiuti watershed has an enormous importance in the development due to its large areal extent and its ability for hosting new settlements. Surface water resources in El-Assiuti watershed need to be optimized by determining the potentiality areas suitable for the RWH. Therefore, an integrated approach involving RS, watershed morphometric analysis and WSPM were vital for addressing such a purpose.

The study demonstrated the suitability of El-Assiuti sub-watersheds for RWH and groundwater recharge. The morphometric parameters included the measurement of linear, areal and relief aspects. Wadi El-Assiuti watershed was distinguished as of the $6^{th}$ order and was subdivided into nine sub-watersheds.

The bifurcation ratio values reflect a nearly homogenous terrain of geologic sediments with moderate structural setting. Drainage density and drainage texture values of the sub-watersheds reflect the low relief and good soil permeability hence highlight its competency for the groundwater recharge by the runoff water. Wadi El-Assiuti sub-watersheds are less than 0.7 (elongation ratio) indicating elongated basins. A map was constructed by the GIS WSPM for determining the RWH potentiality areas based on the morphometric parameters of basin area, basin slope, basin length, drainage density, maximum flow distance, length of overland flow, basin infiltration number, and volume of annual flood. The WSPM model was performed through two scenarios: equal weights to criteria (scenario I), and justified weights based on the sensitivity analysis (scenario II).

The resulted WSPM maps for determining the RWH potentiality areas classified the study area into five potentiality classes ranging from the very low to very high. The two performed WSPMs' scenarios represent a good match in results with respect to the high and very high RWH potentiality classes, which are the most suitable classes for the establishment of different RWH constructions (i.e., storage dams and ground cisterns). These classes are mostly occupied generally by small zones in the northeastern, southeastern and northwestern parts of the wadi, which represent ~ 11.72 % (~723.16 $km^2$) of the total watershed area.

## Acknowledgments

The authors wish to express their great gratitude to the National Authority for Remote Sensing and Space Sciences (NARSS) for providing the facilities needed for conducting the present work.

## REFERENCES

Agarwal, CS., (1998): Study of drainage pattern through aerial data in Nahagarh area of Varanasi district. U.P. J Indian Soc Remote Sens 26:169–175. doi:10.1007/BF02990795.

Aher, PD., Adinarayana, J., Gorantiwar, SD., (2014): Quantification of morphometric characterization and prioritization for management planning in semi-arid tropics of India: a remote sensing and GIS approach. J Hydrol 511:850–860.

AQUAVEO, (2018): Water modeling solutions. Support forum for subwatershed modeling system software (WMS) www.aquaveo.com.

CONOCO (Continental Oil Company), (1987): Geological Map of Egypt (Scale 1: 500,000). CONOCO Inc. in Collaboration with Freie Universitat Berlin, ISBN 3-927541-09-5.

Elewa, H. H., (2008): Prediction of future drawdown of water levels of the Pleistocene aquifer system of Wadi El-Assiuti Area, Eastern Desert, Egypt, as a criterion for management and conservation. Resour Conserv Recycl 52:1006–1014. https://doi.org/10.1016/j.resconrec.2008.03.006.

Elewa, H. H., Qaddah, A. A., El-Feel, A. A., (2012): Determining Potential Sites for Runoff Water Harvesting Using Remote Sensing and Geographic Information Systems-Based Modeling in Sinai. American Journal of Environmental Sciences, Science Publications, USA, Volume 8 No. 1, 2012, 42-55. DOI: https://doi.org/10.3844/ajessp.2012.42.55.

Elewa, H. H., Ramadan, E. M., Nosair, A. M., (2014): Water/land use planning of Wadi El-Arish Watershed, Central Sinai, Egypt using RS GIS and WMS techniques. IJSER 5(9):341–349.

Elewa, H. H., Ramadan, E.M., Nosair, A.M., (2016): Spatial-Based Hydro-morphometric Watershed Modeling for the Assessment of Flooding Potentialities. Environ Earth Sci (2016) 75:927, Springer-Verlag Berlin Heidelberg 2016. (DOI: 10.1007/s12665-016-5692-4). https://link.springer.com/article/10.1007/s12665-016-5692-4

Elewa, H.H. et al., (2018-2020): Water Resources Potentialities for the Central Eastern desert of Egypt, Using RS, GIS and Watershed Modeling Techniques, 320 pp, A Research Project Funded by NARSS.

Elewa, H. H., Nosair, A. M., Ramadan, E. M., (2020): Determination of Potential Sites and Methods for Water Harvesting in Sinai Peninsula by the Application of RS, GIS, and WMS Techniques. Advances in Science, Technology & Innovation – IEREK Interdisciplinary Series for Sustainable Development. Flash Floods in Egypt. Pp. 313-345. © Springer Nature Switzerland AG 2020. ISBN 978-3-030-29634-6 ISBN 978-3-030-29635-3 (eBook). https://doi.org/10.1007/978-3-030-29635-3.

Elewa, H.H., Zelenakova, M., and Nosair, A. M., (2021): Integration of the analytical hierarchy process and GIS spatial distribution model to determine the possibility of rainwater harvesting in dry regions: Wadi Watir of Sinai as a case study. Water 2021, 13(6), 804; https://doi.org/10.3390/w13060804.

ESRI, (2015): ArcGIS 10.4, GIS and mapping software.

Faniran, A., (1968): The index of drainage intensity—a provisional new drainage factor. Aus J Sci 31:328–330.

Feizizadeh, B., Jankowski, P., Blaschke, T., (2004): A GIS based spatiallyexplicate sensitivity analysis approach for multi-criteria decision analysis. Comput Geosci 64:81–95.

Ha, W., Lu, Z., Wei, P., Feng, J., Wang, B., (2012): A new method on ANN for variance-based importance measure analysis of correlated input variables. Struct Saf 38:56–63.

Horton, R. E., (1945): Erosional development of stream and their drainage basin. Hydrogeological approach to quantitative morphology. Bull Geol Soc Am 56:275–370.

Javed, A., Khanday, M. Y., Ahmed, R., (2009): Prioritization of subwatersheds based on morphometric and land use analysis using remote sensing and GIS techniques. J Indian Soc Remote Sens 37:261–274.

Kuldeep, P., Upasana, P., (2011): Quantitative morphometric analysis of a watershed of Yamuna Basin, India using ASTER (DEM) data and GIS. Int J Geomat Geosci 2:248–269. doi:10.12691/ jgg-1-1-7.

Leopold, L. B., Maddock, T., (1953): The hydraulic geometry of stream channels and some physiographic implications: US Geological Survey Professional Paper p 252

Ligmann-Zielinska, A., (2013): Spatially-explicit sensitivity analysis of an agent-based model of land use changes. Int J Geogr Inf Sci 27:1764–1781.

Melton, M. A., (1958): A derivation of Strahler's channel-ordering system. J Geol 67:345–346.

Miller, V. C., (1953): A quantitative geomorphic study of drainage basin characteristic in the clinch, Mountain area, Verdinia and Tennesser, Project NR 389-042, Technical Report 3 Columbia University, Department of Geology, ONR, Geography Branch, New York.

Nag, S. K., (1998): Morphometric analysis using remote sensing techniques in the Chaka Sub-basin, Purulia district, West Bengal. J Indian Soc Remote Sens 26:69–76.

NASA Prediction of Worldwide Energy Resources (Power) Project, (2018): https://power.larc.nasa.gov/.

Obi Reddy, G. P., Maji, A. K., Gajbhiye, K. S., (2002): GIS for morphometric analysis of drainage basin. GIS India, 11 (4): 9-14.

Omara, S., El-Tahlawi, M. R., (1972): Limestone "dykes" in the Nile valley around Assiut Upper Egypt. N jbGeolpataentMnstullgart, pp 473- 483.

Said, R., (1981): The geological evolution of the river Nile. Springer, New York. https://doi.org/10.1007/978-1-4612-5841-4.

Said, R., (1990): The Geology of Egypt. Elsevier, New York.

Saisana, A., Saltelli, A., Tarantola, S., (2005): Uncertainty and sensitivity analysis techniques as tools for the quality assessment of composite indicators. J Royal stat Soc 168:307–323.

Schumm, S. A., (1956): Evolution of drainage system and slope in badlands of Perth Amboy, New Jersey. Bull Geol Soc Am 67:597–646.

Smith, K. G., (1950): Standards for grading textures of erosional topography. Am J Sci 248:655–668.

Strahler, A. N., (1956): Quantitative slope, analysis. Bull Geol Soc Am 67:571–596.

Strahler, A. N., (1964): Quantitative geomorphology of drainage basin and channel network. In: Chow VT (ed) Handbook of applied hydrology. McGraw Hill, New York.

UNESCO, (1965): International hydrological decade Symposium on hydrology of fractured rocks. Dubrovnik (Yugoslavia) Symposium. Paper no. 41, p 13.

USDA-SCS-CN (United States Department of Agriculture-Soil Conservation Service-Curve Number), (1989): Estimating runoff and peak discharges. Chapter 2: in engineering field handbook. http://www.info.usda.gov/CED/ftp/CED/EFH-Ch02.pdf. Accessed 20 Aug 2012.

Van Griensven, A., Meixner, T., Grunwald, S., Bishop, T., Diluzio, M., Srinivasan, R., (2006): A global sensitivity analysis tool for the parameters of multi-variable catchment models. J Hydrol 324:10–23.

Yousef, A. F., (2008): The impact of North West active fault system on the recharge of the quaternary aquifer system around the Nile valley: case study Wadi El-Assiuti, Eastern Desert, Egypt. Eur Water 21(22):41–55.